Severe arterial injury heals with a complex clonal structure involving a large fraction of surviving smooth muscle cells

Gro Grunnet Pløen [a], Charlotte Brandt Sørensen [a], Jacob Fog Bentzon [a,b,*]

[a] *Department of Clinical Medicine, Aarhus University, Aarhus, Denmark*
[b] *Centro Nacional de Investigaciones Cardiovasculares Carlos III (CNIC), Madrid, Spain*

A B S T R A C T

Background and aims: Smooth muscle cell (SMC) lineage cells in atherosclerosis and flow cessation-induced neointima are oligoclonal, being recruited from a tiny fraction of medial SMCs that modulate and proliferate. The present study aimed to investigate the clonal structure of SMC lineage cells healing more severe arterial injury.
Methods: Arterial injury (wire, stretch, and partial ligation) was inflicted on the right carotid artery in mice with homozygous, SMC-restricted, stochastically recombining reporter transgenes that produced mosaic expression of 10 distinguishable fluorescent phenotypes for clonal tracking. Healed arteries and contra-lateral controls were analyzed after 3 weeks. Additional analysis of cell death and proliferation after injury was performed in wildtype mice.
Results: The total number of SMC lineage cells in healed arteries was comparable to normal arteries but comprised significantly fewer fluorescent phenotypes. The population had a complex, intermixed, clonal structure. By statistical analysis of expected *versus* observed fractions of fluorescent phenotypes and visual inspection of coherent groups of same-colored cells, we concluded that >98% of SMC lineage cells in healed arteries belonged to a detectable clone, indicating that nearly all surviving SMCs after severe injury at some point undergo proliferation. This was consistent with serial observations in the first week after injury, which showed severe loss of medial cells followed by widespread proliferation.
Conclusions: After severe arterial injury, many surviving SMCs proliferate to repair the media and form a neo-intima. This indicates that the fraction of medial SMCs that are mobilized to repair arteries increases with the level of injury.

1. Introduction

Recent studies in mouse models have shown that only a small fraction of medial smooth muscle cells (SMCs) contribute to atherosclerotic lesions and flow cessation-induced neointima [1–3]. Depending on the specific model and the size of the analyzed region, the total number of SMCs participating in lesion formation has ranged from 1 to ~10, far less than 1% of the medial SMCs present in the vicinity. The few founder cells proliferate, and many of them lose their contractile phenotype and modulate to fibroblast-like or chondrocyte-like cells in the arterial lesion.

Why only a few of the many SMCs that are present in the media start proliferating in atherosclerosis and flow cessation-induced neointima is

not known [4,5]. One possibility is that of a predetermined subset of medial SMCs with high proliferative potential. Healthy murine aortas contain a Sca1+ subset of partially modulated SMCs with high proliferative capacity that would fit that role [3,6], although Sca1 lineage tracing has not revealed a high degree of contribution of Sca1+ cells in atherosclerosis [7]. In murine pulmonary arteries, a minority subset of Notch3-expressing medial SMCs was found to be the major source of neointimal lesions in pulmonary arterial hypertension [8]. Alternatively, there may be a range in responsiveness among the medial SMCs, potentially leading to greater recruitment at higher levels of stimulation. This principle is known in other cell types, such as endothelial cells [9], and can allow cell populations to respond appropriately to a greater range of stimuli than can be encoded in individual cells [10]. Additional

explanations are possible, as reviewed elsewhere [10,11].

The range in responsiveness theory predicts that more SMCs will participate in remodeling after severe injury than in atherosclerosis or flow cessation. Severe mechanical injury leads to disruption of the extracellular matrix, including the elastic laminae, increases in growth factors and cytokines that are released from the damaged matrix or secreted from incoming thrombocytes and immune cells, and loss of the inhibitory signals from endothelial cells [12–15]; all stimuli that may trigger the threshold for modulating and dividing in a higher fraction of SMCs. To test this prediction, we studied the clonal structure of neo-intimal SMCs after severe mechanical injury in the murine carotid artery. We found that severely injured arteries heal with a complex clonal architecture involving a much larger fraction of available SMCs than in previously characterized disease models with milder arterial injury.

2. Materials and methods

2.1. Animals

Myh11-CreER^{T2} mice (B6.FVB-Tg[Myh11-cre/ERT2]1Soff/J, The Jackson Laboratory), expressing tamoxifen-inducible Cre recombinase under the SMC-specific Myh11 promoter, were crossed with Confetti mice (B6.129P2-Gt[ROSA]26Sortm1[CAG-Brainbow2.1]Cle/J, The Jackson Laboratory) that harbor a stochastic multicolor Cre recombinase reporter in the Rosa26 locus. Strains had been backcrossed to the B6 strain (C57BL/6N or C57BL/6J) for at least 6 generations. The Confetti transgene expresses membrane-bound cyan fluorescent protein (CFP), nuclear green fluorescent protein (GFP), yellow fluorescent protein (YFP), or red fluorescent protein (RFP) upon recombination. Mice were intercrossed to obtain experimental animals homozygous for the Confetti allele yielding 10 possible fluorescent phenotypes (GFP, GFP/CFP, GFP/YFP, GFP/RFP, CFP, CFP/YFP, CFP/RFP, YFP, YFP/RFP, and RFP). Only males were used in the experiments because the Myh11-CreER^{T2} transgene is inserted on the Y chromosome. Recombination was induced at 7 weeks of age with a 5-day series of 2 mg/day i.p. of tamoxifen (T5648, Sigma) dissolved in corn oil. Wildtype B6 (C57BL/6JRj) mice were obtained from Janvier.

2.2. Triple-injury

Arterial injury was induced in 9-week-old male Myh11-CreER^{T2}-Confetti (n = 9) and wildtype mice (n = 18) using a previously described triple-injury technique [16]. Mice were anesthetized with sevoflurane (induction 4%, maintenance 2–3%), injected with buprenorphine (0.1 mg/kg, s.c.) for analgesia, and placed in a supine position on a heating pad. The depth of the anesthesia was checked regularly by the pedal withdrawal reflex. The surgical area was shaved and disinfected. A cervical midline incision was made, and the right common carotid artery (CCA), the internal carotid artery (ICA), and the external carotid artery (ECA) were dissected free from surrounding tissue. The ECA was ligated as distal as possible, the ICA was ligated just distal to the bifurcation, and the CCA closed as proximal as possible with a microvascular clamp. A hole was cut in the ECA through which a nylon wire (Ø: 0.18 mm) was inserted and moved up and down 4 times to remove the endothelium. The same hole was subsequently used to insert a 30G needle connected to an Atrion QL Inflation device (Atrion Medical, QL2530, #96402). A temporary ligature proximal to the superior thyroid artery (STA) was used to fix the needle and seal the CCA before inflation with saline (1 bar, 20 s). After removal of the suture and needle, the ECA was ligated proximal to the hole, though distal to the STA. This leaves the STA as the only outflow tract, reducing blood flow through the CCA. After removing the microvascular clamp, blood flow in the STA was confirmed before closing the wound with a 6-0 suture. For postoperative analgesia, drinking water was supplemented with buprenorphine (0.01 mg/mL) for 3 days. Myh11-CreER^{T2}-Confetti mice (n = 9) were terminated 3 weeks after triple-injury. Wildtype mice received a single injection (50

mg/kg, s.c.) of EdU (BCK488-IV-IM, Sigma) at 24h before termination and were terminated 1 (n = 6), 3 (n = 6) or 7 (n = 6) days after triple-injury. Briefly, mice were anesthetized by intraperitoneal injection of pentobarbital (250 mg/kg) and lidocaine (20 mg/kg), perfused with cardioplex (30 s) and 4% phosphate-buffered formaldehyde (5 min) at 100 mmHg through the left ventricle, followed by immersion-fixation in 4% phosphate-buffered formaldehyde for 24h. Uninjured left carotid arteries were used as controls to study normal arterial structure and Confetti recombination (n = 6).

2.3. Tissue processing

The carotid arteries were excised and cryoprotected in sucrose solutions (25% for 24h and 50% for 24h), embedded in OCT compound, and snap-frozen with liquid nitrogen. Five μm thick cross-sections were obtained from the bifurcation in 9 levels, each 500 μm apart (0–4000 μm). In arteries from Myh11-CreER^{T2}-Confetti mice, sections from each level were stained with DAPI or Orcein, using standard protocols, and mounted for microscopy. Two adjacent sections from three levels of each carotid were selected for immunofluorescence. Those sections were stained for Acta2 and Sox9, using rabbit monoclonal anti-Acta2 (abcam, ab32575, 1:200) or rabbit polyclonal anti-Sox9 (abcam, ab185230, 1:200), followed by Alexa 647–conjugated donkey anti-rabbit (abcam, ab150075, 1:400) secondary antibody. In arteries from wildtype mice, sections from the 500 μm level were stained for EdU-labeled proliferating cells according to the manufacturer's recommendation (BCK488-IV-IM, Sigma).

2.4. Microscopy

Images were obtained using a Zeiss Laser Scanning Confocal Microscope equipped with a C Apochromat 40x/1.2 water objective and differential interference contrast III optics. The entire vessel was scanned by automated stitching of 3x3 images, acquired with 4 sequential captures. First, the 514 nm and 633 nm lasers were used to simultaneously acquire the YFP and far-red (autofluorescence or Acta2/Sox9 stain). Second, GFP and EdU (6-FAM-Azide) were imaged with a 488 nm laser. Third, the CFP and RFP channels were acquired with 458 nm and 543 nm lasers, respectively. Finally, DAPI was imaged with a 405 nm laser. All acquisition and postprocessing settings were tested with sections from fluorescent negative female controls to confirm specificity. ZEN Black 2.3 software was used for image acquisition, and ZEN 3.6 Blue was used to quantify recombination outcomes, areas, number of SMC profiles, and cellularity. Nucleated cells with expression of each of the Confetti colors were counted in a single z-layer of entire cross-sections for the determination of recombination efficiency and the statistical testing for clonality (see below). For the manual evaluation of clonality, clones were recognized by the immediate proximity of at least 5 cells of the given phenotype, including fluorescence-positive cell profiles without a nucleus. Maximum intensity projection of 3 z-stack images of Acta2 and Sox9 were composed for the publication (1.67 μm in total). Brightness and contrast were adjusted to enhance the visibility of the fluorescent signal in all the publication images.

2.5. Statistical analysis

All statistical tests were performed in Prism 9.3.1 (GraphPad Software). $p < 0.05$ was considered statistically significant. Statistical differences between specific levels and controls were analyzed by Kruskal-Wallis with Dunnett's test. Bars in dot plots represent mean ± SD.

To identify cells belonging to a clone, we performed stepwise statistical testing. In the first step, we determined the 95% confidence interval upper limit for the recombination rate of the Confetti phenotypes observed in the healthy controls. These values constituted the "probability of success" for each phenotype (p^k) used in the subsequent binominal testing of observed phenotypes in the individual samples. For each

fluorescent phenotype of cells in a section of healed artery, we then calculated the probability that the observed number of k cells of that phenotype was the result of random recombination in n cells, where n is the total number of Confetti$^+$ cells in the given section. The probability was calculated using the binomial distribution as $P(X \geq k) = \sum_k^n \binom{n}{k} p^k (1-p)^{n-k}$. The statistical significance of $p < 0.05$ was Bonferroni-corrected ($p < 0.05/b$) according to the number of tests (b) performed in each step. If the probability for one or more of the fluorescent phenotypes was lower than the Bonferroni-adjusted threshold, cells with those fluorescent phenotypes were accepted as clones and subsequently removed from the analysis. The residual fluorescent cells were then re-analyzed as if sections came from mice that could not recombine to the fluorescent phenotypes already accepted as clones. This involved upscaling the 95% confidence intervals for recombination rates of the residual fluorescent phenotypes to keep the total rate constant. The analysis above was then repeated, and the iterative process was continued until no residual fluorescent phenotype exceeded the Bonferroni-corrected threshold or all residual phenotypes contained less than 5 nucleated cells.

2.6. Study approval

The Danish Animal Experiments Inspectorate approved animal procedures, which were all conducted at the Department of Clinical Medicine, Aarhus University according to national regulatory standards (approval no. 2020-15-0201-00410).

3. Results

3.1. Recombination outcomes in homozygous Myh11-CreER^{T2}-Confetti mice

We examined the distribution of the different recombination outcomes (Fig. 1A) in medial SMCs in uninjured left carotids from 6 homozygous Myh11-CreER^{T2}-Confetti male mice at 4 weeks after tamoxifen injections. Fluorescence was present in 86.9% ± 6.34% (mean ± SD) of medial SMCs (Fig. 1B and C). Expression of RFP was the most common outcome of recombination, followed by CFP, YFP, and GFP. This distribution was consistent with previous reports [1,2], but the total fraction of fluorescent cells was higher, presumably explained by each cell having two alleles of the Confetti transgene. Combinations
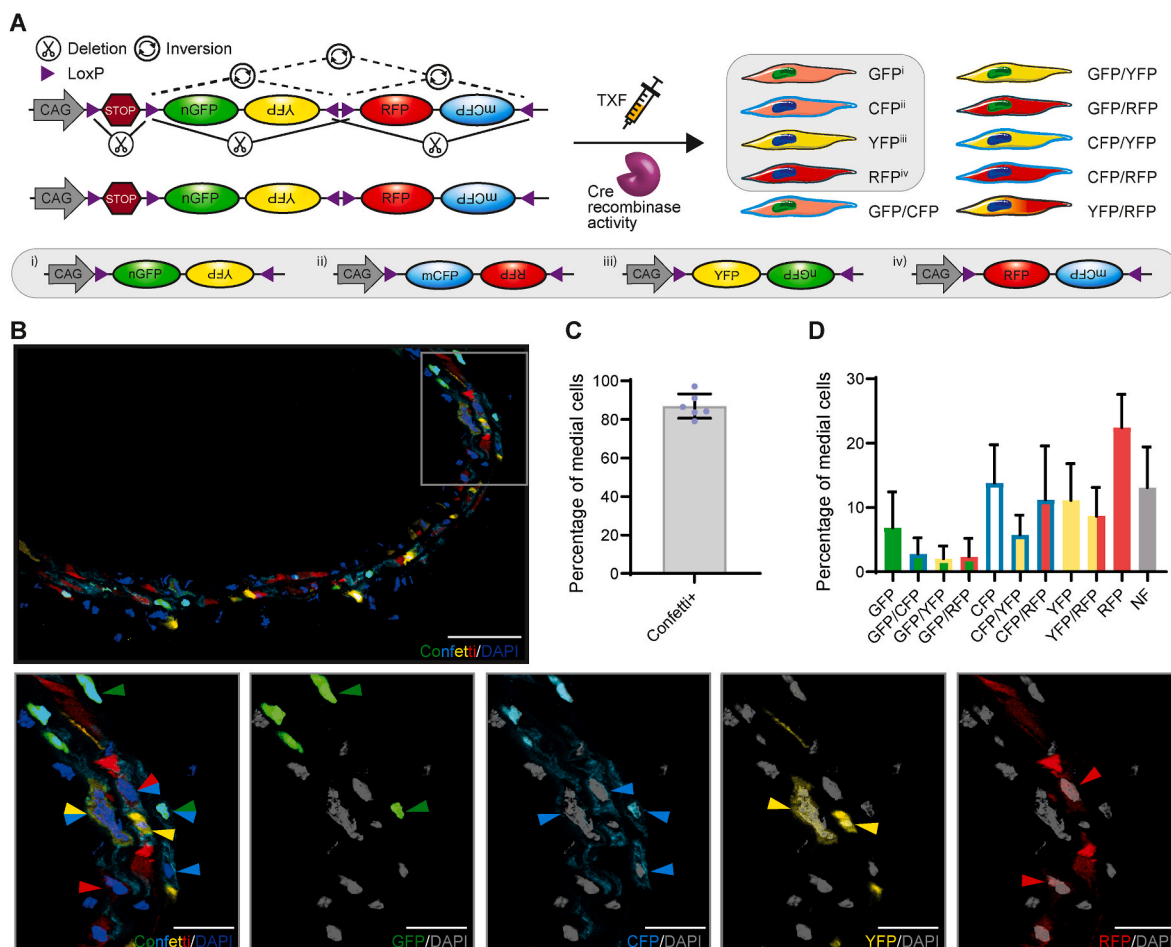

Fig. 1. Mosaic fluorescent protein expression in smooth muscle cells.
(A) Schematic representation of the homozygous Confetti$^+$ reporter yielding 10 possible recombination outcomes. Grey boxes mark the 4 possible recombination outcomes achievable for a single Confetti allele in hemizygous animals. Stochastic recombination of both alleles in homozygous animals enables the detection of the additional 6 double fluorescence-positive phenotypes. TXF, tamoxifen. (B) Representative example of a carotid artery section analyzed by confocal microscopy. Higher magnification views of the region marked in A (grey box) are shown underneath. The images show the combined fluorescent signal and the individual fluorescent channels. DAPI is depicted in either blue or grey. (C) Total percentage of cells expressing fluorescent protein in 765 nucleated medial SMCs profiles in uninjured carotid arteries from 6 homozygous Myh11-CreER^{T2}-Confetti mice. (D) Average percentage-wise distribution of the 10 possible fluorescent phenotypes. GFP, green fluorescent protein; CFP, cyan fluorescent protein; YFP, yellow fluorescent protein; RFP, red fluorescent protein; NF, non-fluorescent. Data are shown as mean ± SD or mean + SD. Scale bars are 50 μm (upper panel) and 20 μm in the magnified region (lower panel). (For interpretation of the references to color in this figure legend, the reader is referred to the Web version of this article.)

of the recombination outcomes of the homozygous Confetti transgenes yielded 10 distinguishable phenotypes, which provide higher certainty in determining clonality than can be achieved with the 4 phenotypes encoded by the hemizygous transgene. The distribution of the 10 individual phenotypes is shown in Fig. 1D.

3.2. Neointima induced by triple-injury to the carotid artery

The experimental design is shown in Fig. 2A. Nine homozygous Myh11-CreER^T2-Confetti male mice were recombined with tamoxifen injections at 7 weeks of age. Two weeks later, we subjected the right carotid artery to a triple-injury procedure that combines endothelial denudation, arterial distension, and reduced blood flow (Fig. 2B). This technique has previously been shown to induce neointima in the B6 strain [16], which is relatively resistant to injury-induced intimal hyperplasia by other methods [17]. Three weeks after surgery, the animals were killed and perfusion fixed, and the carotid arteries were cryo-sectioned at 9 levels with 500 μm spacing that were examined for neointima formation by microscopy (Fig. 2C). Neointima was most pronounced at 500–2500 μm from the carotid bifurcation and these 5
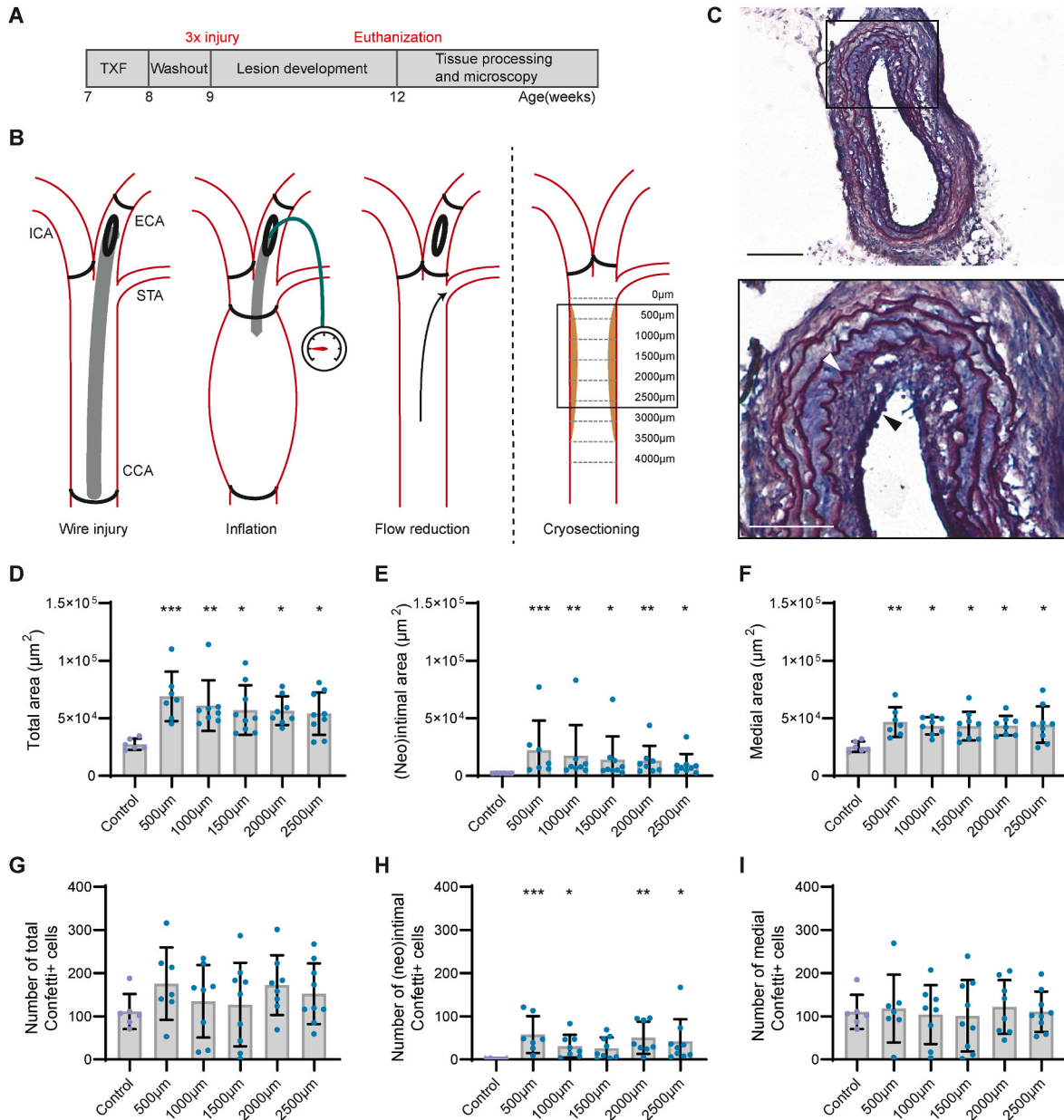

Fig. 2. Triple-injury procedure and lesion analysis.
(A) Experimental design of the study. (B) Schematic representation of the triple-injury procedure, consisting of endothelial denudation, mechanical stretch, and flow alteration. The developed lesions were sectioned at 9 levels (grey dashed lines) and 5 levels (500–2500 μm) were selected for quantification (black box). (C) Orcein staining from a representative section (500 μm). The black outlined region is magnified, and the neointima is marked with a black arrow from the luminal and a white arrow from the medial side. Scale bars are 100 μm for whole carotid and 50 μm in the magnified region. (D–F) Total, (neo)intimal and medial areas were significantly increased compared to the control. (G–I) The number of Confetti⁺ cells was increased in the neointima compared to the control intima, which contained very few SMCs, and remained constant in the media. One sample had a profound increase in neointimal area, probably representing a revascularized thrombus. Data points are missing from four sections that were of inadequate quality. Data are shown as mean ± SD. Asterisks indicate the statistical difference between specific levels and the control, analyzed by Kruskal-Wallis with Dunnett's test ($*p < 0.05$, $**p < 0.005$, $***p < 0.0005$). ICA, internal carotid artery; ECA, external carotid artery; STA, superior thyroid artery; CCA, common carotid artery.

levels were further analyzed for clonal structure.

3.3. Clonal structure of neointima and media

Confocal microscopy for the Confetti colors displayed clear disruption of normal arterial media structure and the formation of neointima. Both the intimal and medial areas were significantly increased in the injured arteries compared to the control arteries (Fig. 2D–F). The formation of neointima was accompanied by a significant increase in the number of Confetti$^+$ cells in the intima, as expected, whereas the number of medial Confetti$^+$ SMC was comparable between samples and control (Fig. 2G–I). Confetti$^+$ cells accounted on average for 46.3% of all nucleated cell profiles in sections, but the percentage in individual sections was highly variable with some sections having few and others almost exclusively fluorescent SMC-derived cells (SD: ± 23.66%). It should be noted that part of the non-fluorescent cells may still be SMC-derived because recombination among medial SMCs was not complete, but since they cannot be distinguished in our analysis from other cell types, such as macrophages and fibroblasts, they were not considered.

To understand whether healing of the arterial injury involved mono-, oligo- or polyclonal growth, we counted the number of different Confetti$^+$ phenotypes in each section. There was an overall reduction in the number of the 10 possible phenotypes of SMCs in sections at all levels of the lesions (4.37 ± 2.06, mean ± SD), compared with controls (9.17 ± 0.98, mean ± SD). The neointima in each section contained on average 2.07 different phenotypes (SD: ± 1.82) (Fig. 3A and B). The decline of different fluorescence phenotypes combined with the increased (in intima) or unaltered (in media) number of SMC-derived cells indicated that clonal proliferation of a limited number of founder cells repairs the artery. Some clones were distinct same-colored patches, but many sections showed more complex patterns with intermixing of 2 or more fluorescent phenotypes in a region. Examples are shown in Fig. 3C–E.

The complex clonal architecture of the SMC-derived population precluded simple counting of same-colored patches as a way of analyzing clonality. Instead, we designed a statistical stepwise approach that did not rely on the spatial distribution of cells. For each of the fluorescent phenotypes in a section (e.g., 77 RFP/YFP among 200 total Confetti$^+$ cells in Fig. 3C), we calculated the probability that it had resulted from random recombination of the Confetti transgene without subsequent cell proliferation. These probabilities were calculated from the binomial distribution using the upper limits of the 95% confidence intervals for the recombination rate of the fluorescent phenotypes observed in normal arteries (from Fig. 1D). If the probability for one or more of the phenotypes was lower than the Bonferroni-corrected significance threshold, cells with those phenotypes were accepted as clones. Cells with the phenotypes accepted as clones were then removed, and the analysis was repeated to test if any of the residual fluorescent phenotypes constituted more of the residual Confetti$^+$ cells than could be explained by the outcome of recombination without cell proliferation. These steps were repeated until no fluorescent phenotype exceeded the threshold or the residual groups contained less than 5 cells per phenotype. This yielded 118 clones identified in 41 sections of injured arteries and none in the normal arterial wall. The advantage of the statistical approach is that clones that are mixed can still be recognized, but it was also clear that the approach missed some clonal populations, which could only be recognized by their spatial proximity (example in Fig. 3F). Therefore, the remaining phenotypes that were not considered to be clonal in the statistical approach were examined manually for spatial proximity. The criteria set for a clonal population was the immediate proximity of at least 5 cells of the given phenotype, including fluorescence-positive cell profiles without a nucleus. That yielded an additional 15 clones resulting in 133 clones for further analysis. It should be noted that some of these clones may be the same clone spanning the 500 μm from one examined level to the next.

Clones differed widely in size with an average of 46 cells/clone (SD: ± 46.7, range: 5–258 nucleated cells in a section) (Fig. 3G). Most clones

were small, but some accounted for up to 67% of the total amount of counted cells in a section. The average clone size was 29.5% of Confetti$^+$ cells in a section (SD: ± 25.3%) (Fig. 3H). When analyzing only the dominant clone from each section, the average size was 93 cells/clone (SD: ± 56.8, range: 11–258 cells), representing 28.1–100% of the Confetti$^+$ cells per section (mean: 61.7%, SD: ± 20.0%) (Fig. 3I). Importantly, only 1.6% of Confetti$^+$ cells (100/6191) did not show evidence of being part of a clonal population.

3.4. Architecture of clones

Among the 133 identified clones, 104 were observed to span neointima and media. Two clones were only detected in the neointima and 27 were observed only in the media (Fig. 4A). The 104 spanning clones were analyzed for their relative presence in the neointima and media. Overall, we observed that most clones had a predominance of cells in the media (Fig. 4B). An example of an RFP$^+$ clone, spanning neointima and media, predominately located in the media is shown in Fig. 4C.

3.5. The fate of clonal SMCs after triple-injury in homozygous mice

In each mouse, two adjacent sections from 3 levels with high numbers of Confetti$^+$ cells were analyzed by immunofluorescence for the SMC subtype markers Acta2 and Sox9. Acta2 marks cells with partially preserved contractile SMC phenotype, and Sox9 cells that have lost SMC phenotype and acquired full or partial chondrocyte-like phenotype [2]. These subtypes are on each end of the spectrum of phenotypes observed in atherosclerosis by single-cell RNA sequencing [18]. Acta2$^+$ cells were found in 27/27 analyzed sections, with the highest intensity in the neointima. Sox9$^+$ cells were detected in 22/27 sections in the media, but only 13/27 sections in the neointima. Comparing the adjacent sections, we often observed Acta2 and Sox9 to be expressed by the same clone (Fig. 4D and E).

3.6. Cell loss and proliferation in early lesion development

The clonal structure of healed injured arteries indicated that the early stages of injury and repair must have involved a massive loss of medial SMCs followed by widespread proliferation among the surviving cells. To explore this, we performed triple-injury in 3 groups of wildtype mice and analyzed arteries 1, 3, and 7 days after injury (n = 6 in each group). Representative images from uninjured and injured arteries are shown in Fig. 5A. The number of medial cells decreased substantially by 77% at day 1 before returning to normal numbers after 7 days (Fig. 5B). Intimal cells were also initially lost, consistent with endothelial denudation (Fig. 5C).

For an overall assessment of the dynamics of cell proliferation, we marked cells in S phase with a pulse of EdU injected 24h prior to termination. No labeled cells were detected in uninjured controls and numbers were low at day 1. In both the media and intima, the fraction of proliferating cells was the highest at day 3, where it reached a mean of 7.2% (SD: ± 3.0%) in the arterial media (Fig. 5D and E). Notably, since the half-life of EdU in mice is short and the S phase estimated to be around 7 h in SMCs [19], the fraction of SMCs in the cell cycle may be > 3 times higher than the EdU$^+$ fraction if proliferation is asynchronous.

4. Discussion

Tools to study the clonal architecture of cell lineages have provided new insight into the mechanisms that underlie recruitment and proliferation of SMCs in arterial disease [4,5]. Previous experiments with stochastically recombining fluorescence Cre reporters showed that only a small subset of medial SMCs proliferates in atherosclerosis and after flow cessation, while most remain dormant [1–3,20]. It remains to be determined if the clonal potential of SMCs is predetermined among medial SMCs or depends on the stimulus. Here we studied the
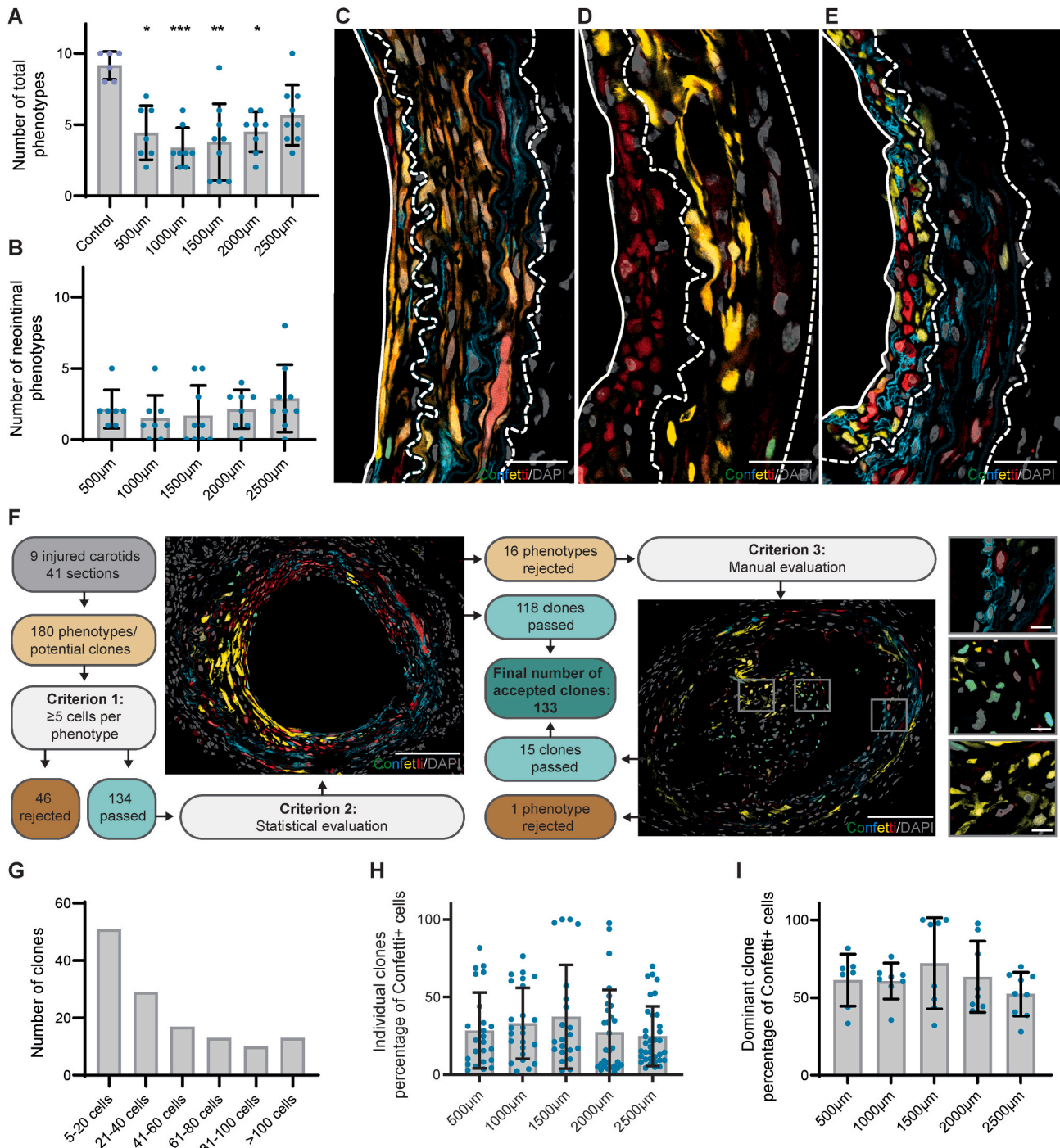
Fig. 3. Confetti$^+$ phenotypes observed in the injured arteries and the definition and evaluation of Confetti$^+$ clones.

(A) The number of cells with the 10 possible fluorescent phenotypes observed in each section at the five examined levels. The number was significantly decreased compared with control arteries at four of the five levels (500–2000 μm). The number of phenotypes at each level was compared to the control with Kruskal-Wallis with Dunnett's test (*$p < 0.05$, **$p < 0.005$, ***$p < 0.0005$). (B) The neointima typically contained few different fluorescent phenotypes (mean: 2.1). Data points are missing from four sections that were of inadequate quality. Data are shown as mean ± SD. (C–E) Confocal microscopy examples of injured arteries with different clonal structures: the same dominant phenotype (RFP/YFP) in neointima and media in C, separate phenotypes mainly located in the media (YFP) and intima (RFP) in D, and media and neointima displaying three intermixed phenotypes of SMCs (YFP, RFP, and CFP) in E. Signals for fluorescent proteins and DAPI (grey) are shown. GFP, green fluorescent protein; CFP, cyan fluorescent protein; YFP, yellow fluorescent protein; RFP, red fluorescent protein; luminal surface of neointima marked by a solid white line, dashed white lines define medial boundaries. Scale bars 25 μm. (F) Flowchart representing the selection process of Confetti$^+$ cells. Sections from 5 levels (500–2500 μm) of 9 injured arteries were selected for analysis. Four sections were excluded because of inadequate quality. 180 phenotypes/potential clones were observed. All clones had to pass a size criterion (≥5 cells/phenotype) and either a statistical evaluation or manual evaluation. The left image illustrates a section that passed the statistical approach. The right image illustrates a section that failed the statistical but passed the manual evaluation. The analysis resulted in 133 Confetti$^+$ clones. Scale bars 100 μm and 10 μm in the magnified regions. (G) The 133 determined clones varied widely in size. (H) The percentage-wise size of clones (out of all Confetti$^+$ cells) at each examined level. (I) The percentage-wise size of the dominant clone (out of all Confetti$^+$ cells). Data are shown as mean ± SD. (For interpretation of the references to color in this figure legend, the reader is referred to the Web version of this article.)
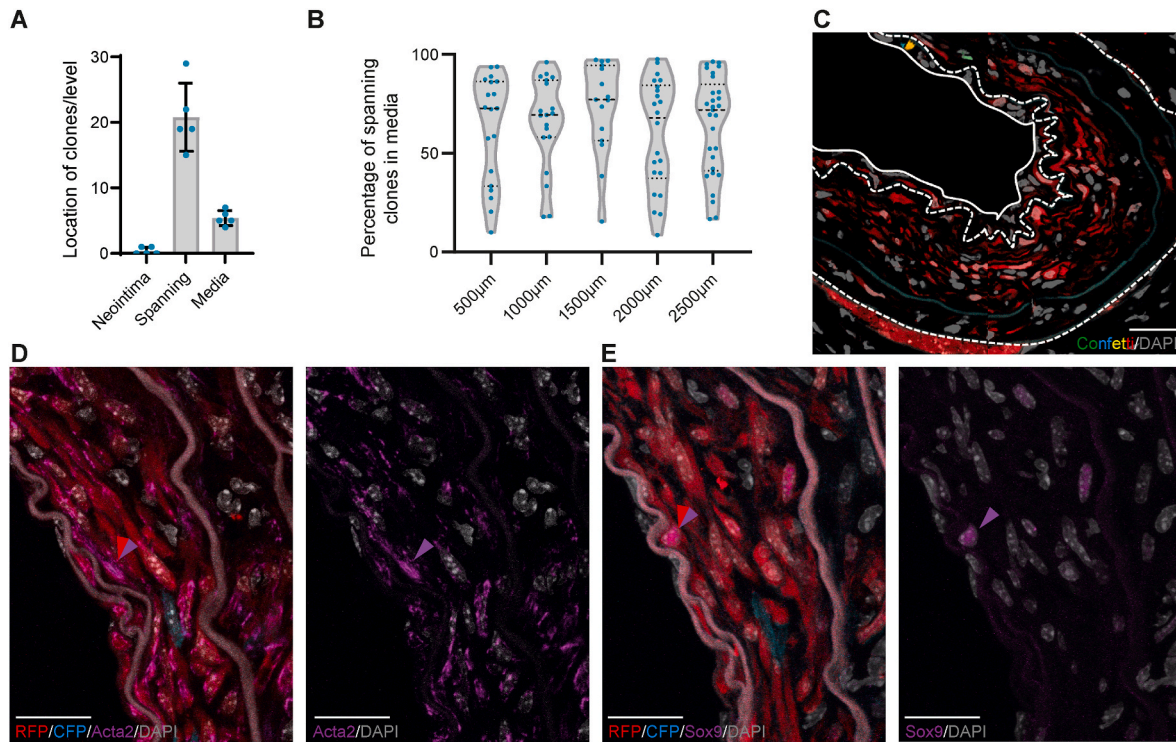
Fig. 4. The location of Confetti⁺ clones.
(A) Assessment of the intra-arterial location of the 133 identified clones (mean ± SD). Clones spanning the neointima and media were the most frequent, accounting for 104 of the clones. (B) Violin-plot showing the cellular distribution of the 104 spanning clones between the neointima and media at each level. The majority of clones presented a higher percentage of the cells located in the media. (C) Confocal microscopy example of an RFP positive clone spanning the neointima and media, with the majority of cells located in the media. Luminal surface marked with a solid white line; dashed lines mark medial borders. (D–E) Adjacent sections of an injured carotid were stained for Acta2 and Sox9 and maximum intensity projections are shown. The same RFP positive clone (red arrows) contained both Acta2 and Sox9 positive cells (purple arrows). Scale bars are 25 μm in C and 20 μm in D-E. (For interpretation of the references to color in this figure legend, the reader is referred to the Web version of this article.)
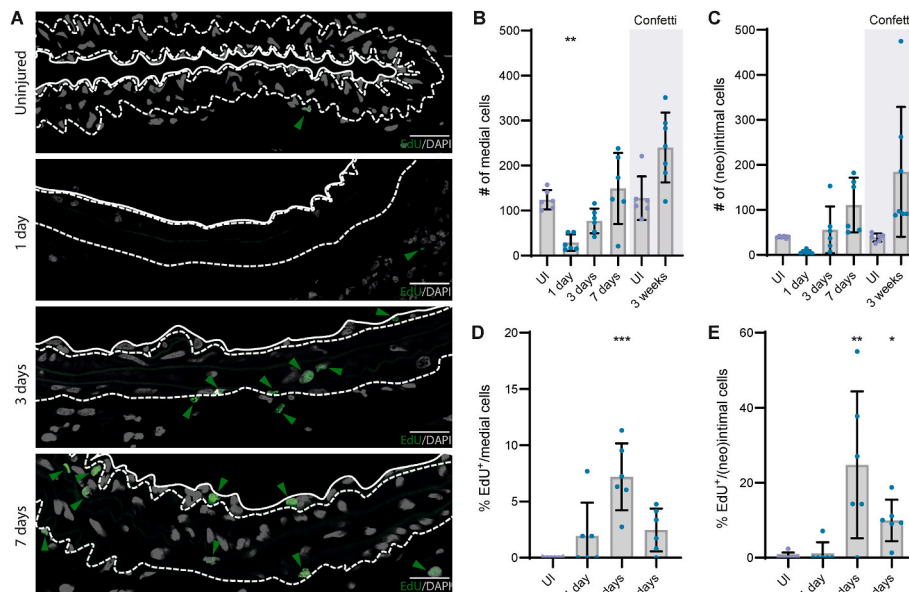

Fig. 5. Evaluation of early changes in carotid arteries after the triple-injury procedure.
(A) Representative images from carotid arteries harvested from wildtype mice at 1, 3 or 7 days post triple-injury. Uninjured left carotids from day 1 were used as controls (n = 6 in all 4 groups). Green nuclear signal represents EdU labeled cells. (B–C) Number of medial and (neo)intimal cells counted in sections at 1, 3 and 7 days after the triple-injury procedure. For comparison, the graphs include data from the same level of the carotid from the Myh11-CreER^{T2}-Confetti mice at 3 weeks post triple-injury (marked with purple background). (D–E) Fraction of medial and (neo)intimal cells in S phase as determined by a single EdU injection administered 24h before sacrificing the animals. Cell numbers and EdU⁺ cells at each timepoint were compared to the uninjured (UI) control with Kruskal-Wallis with Dunnett's test (*$p < 0.05$, **$p < 0.005$, ***$p < 0.0005$). Data are shown as mean ± SD. (For interpretation of the references to color in this figure legend, the reader is referred to the Web version of this article.)

architecture of SMCs healing more severe mechanical injury than previously investigated. In this context where there is a substantial loss of SMCs and disruption of the arterial layers, we found that a large fraction of the surviving SMCs contributes to small or large cellular clones in the media and intima (Fig. 6).

These findings fit previous observations of widespread SMC proliferation after balloon injury to arteries [21]. Clowes et al. found that denuding and distending balloon injury inflicted on carotid arteries in rats was followed by a burst in medial SMC proliferation [21]. Approximately half of surviving medial SMCs passed through S phase within 2 days [21]. Proliferation continued as long as the endothelium had not regenerated, but the numbers of SMCs plateaued after 2 weeks, indicating that proliferation was offset by continuous SMC death [21]. These careful observations in the early phases of arterial neointima formation have been difficult to reconcile with the mono- or oligoclonal structure that characterizes neointimal and atherosclerotic lesions in previously analyzed mouse models [1–3].

By inflicting denuding and distention injury, the triple-injury technique that we applied in the mouse carotid resembles balloon injury. Importantly, the clonal structure we saw was also consistent with the SMC behavior described by Clowes et al. [21]. First, we found evidence that almost all SMCs after 3 weeks of arterial remodeling belonged to a clone of same-colored cells, indicating that nearly all SMCs surviving to 3 weeks after the injury had undergone proliferation. Second, the clones were typically rooted in the arterial media indicating that the founders were early proliferating SMCs that subsequently extended their progeny to the developing overlaying intima, rather than SMCs migrating to the intima before proliferating there.

The main difference in the SMC response after severe arterial injury compared with flow cessation-induced neointima or early atherosclerosis is not in the number of founders that undergo clonal proliferation, which also in our studies were limited because relatively few medial cells survived the injury. It is the number of cells that are *not* activated that is vastly different. The arterial media is intact after flow cessation and beneath small atherosclerotic lesions, but only a small fraction of the many available medial SMCs start proliferating and form clones [1–3,20]. Yet 3 weeks after triple injury, there is not a persistent population of medial SMCs with a mosaic fluorescent protein expression pattern that has not proliferated. This context-dependency of SMC responses speaks against the existence of a fixed subset of SMCs that are primed to repair an arterial injury. If repair depended on such a finite population, part of which would be lost due to the high level of injury, one may have expected an even simpler clonal structure than in models where most cells survive. Rather, the observations indicate that the fraction of medial SMCs responding to injury increases with the strength and extent of the mitogenic stimulus.

After triple-injury, this strong stimulus is provided by several mechanisms. Normal medial SMCs have a very low rate of proliferation,

which is partly instructed by outside-in signaling through integrins binding to the pericellular matrix [13]. Disruption of these cellular connections by the mechanical injury, release of growth factors from activated platelets and immune cells (e.g., PDGF), and loss of inhibitory factors from the missing endothelium (e.g., NO) are all stimulants for SMC proliferation [14]. The damage may also release growth factors that are sequestered in the extracellular matrix [15]. Through these multiple mechanisms, the fraction of local SMCs that respond by entering the cell cycle may be scaled to the severity of the injury. In that context, it is interesting to note that recent studies on atherosclerosis also indicate that the fraction of SMCs responding in vascular disease is a regulatable trait, which may depend on instructions from recruited immune cells, including TNF release, and is increased with aging [22].

Our studies were not aimed at mapping SMC-derived cellular subtypes after injury, but we did note that SMC-derived cells after severe injury encompassed both contractile Acta2$^+$ cells and Sox9$^+$ chondromyocytes, which are at the opposite ends of the spectrum of diversity in murine atherosclerotic lesions [2,23]. Yet in injured arteries, chondromyocytes were mainly located in the media, whereas in atherosclerosis, they are residing in intimal plaque [2,23]. The presence of chondromyocytes after arterial injury is consistent with a recent comparative scRNA-seq analysis which found that injury induces types of SMC-derived cells that are similar to those found in atherosclerosis [24].

4.1. Strengths and weaknesses

An advantage of the present study is the use of homozygous Confetti mice for visualizing complex clonal structures. Yet, because of the complexity of the clonal structure, an even higher number of separate labels, such as those that can be achieved by barcoding and sequencing [25], would have been necessary for precise estimates of clone number. Such approaches, however, do not provide the spatial information provided by microscopy. Because of the complex intermixed clonal structure, techniques commonly used to delineate simple clonal structures, such as manual delineation of same-colored patches [1–3], were not applicable. Therefore, we developed a step-wise statistical approach that in each step tested whether the distribution of cellular fluorescent phenotypes deviated significantly from what would be expected if cells were randomly drawn from the distribution of fluorescent phenotypes observed in normal arteries. The approach was supplemented by manual evaluation of missed clones and a lower limit of 5 cells/clone. While we consider this approach robust in identifying cells with evidence for having divided, it cannot determine the exact number of SMC-derived clones along the artery. Some phenotypes are common (e.g., RFP), and the potential merging of clones with the same phenotype cannot be excluded. Furthermore, clones identified at different levels may well be large clones extending more than 500 μm along the artery. For that
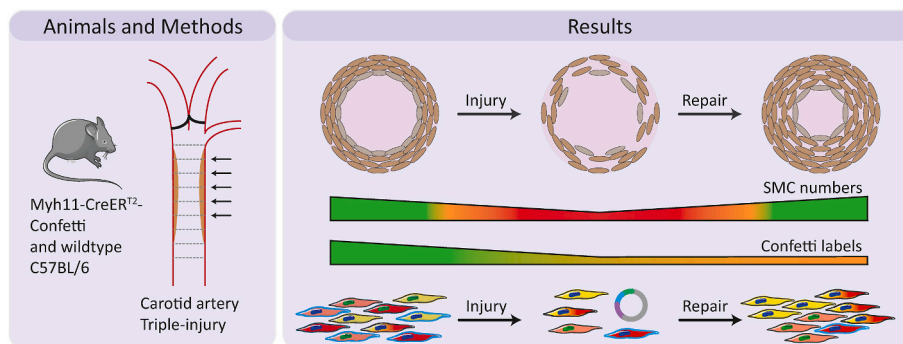

Fig. 6. After severe arterial injury, many surviving SMCs proliferate to repair the media and form a neointima. This is different from models of atherosclerosis and flow cessation-induced neointima, where few SMCs respond, and indicates that the fraction of medial SMCs mobilized to repair arteries increases with the level of injury.

reason, we make no conclusions as to the number of founders that proliferate to heal the injury in the triple-injury model, but only that there are few cells that do not participate.

4.2. Conclusion

In conclusion, we propose that SMC injury response is merely mono/oligoclonal in situations of mild injury, whereas severe injury provokes proliferation in a greater subset of medial SMCs. More research is needed to understand the responsible mechanisms. Multiple regulators of arterial SMC proliferation and neointima formation after injury have been identified, and it has been shown that the magnitude of the response varies widely among different murine genetic backgrounds [17]. For many factors, including genetic background, it is not clear whether they control the fraction of SMCs that enter the cell cycle or the rate of subsequent proliferation. Reassessing key regulators and the impact of genetic background in studies that incorporate clonal tracking techniques could be important to resolve these questions.

Financial support

CRediT authorship contribution statement

Gro Grunnet Pløen: Conceptualization, Methodology, Investigation, Formal analysis, Visualization, Writing – original draft, Writing – review & editing. **Charlotte Brandt Sørensen:** Supervision, Writing – review & editing. **Jacob Fog Bentzon:** Conceptualization, Formal analysis, Supervision, Writing – review & editing.

Declaration of competing interest

The authors declare that they have no known competing financial interests or personal relationships that could have appeared to influence the work reported in this paper.

Acknowledgments

References

[1] J. Chappell, J.L. Harman, V.M. Narasimhan, et al., Extensive proliferation of a subset of differentiated, yet plastic, medial vascular smooth muscle cells contributes to neointimal formation in mouse injury and atherosclerosis models, Circ. Res. 119 (2016) 1313–1323, https://doi.org/10.1161/circresaha.116.309799.

[2] K. Jacobsen, M.B. Lund, J. Shim, et al., Diverse cellular architecture of atherosclerotic plaque derives from clonal expansion of a few medial SMCs, JCI Insight 2 (2017), e95890, https://doi.org/10.1172/jci.insight.95890.

[3] M.D. Worssam, J. Lambert, S. Oc, et al., Cellular mechanisms of oligoclonal vascular smooth muscle cell expansion in cardiovascular disease, Cardiovasc. Res. 119 (2023) 1279–1294, https://doi.org/10.1093/cvr/cvac138.

[4] A. Misra, R. Rehan, A. Lin, et al., Emerging concepts of vascular cell clonal expansion in atherosclerosis, Arterioscler. Thromb. Vasc. Biol. 42 (2022) e74–e84, https://doi.org/10.1161/ATVBAHA.121.316093.

[5] M.D. Worssam, H.F. Jørgensen, Mechanisms of vascular smooth muscle cell investment and phenotypic diversification in vascular diseases, Biochem. Soc. Trans. 49 (2021) 2101–2111, https://doi.org/10.1042/bst20210138.

[6] L. Dobnikar, A.L. Taylor, J. Chappell, et al., Disease-relevant transcriptional signatures identified in individual smooth muscle cells from healthy mouse vessels, Nat. Commun. 9 (2018) 4567, https://doi.org/10.1038/s41467-018-06891-x.

[7] H. Wang, H. Zhao, H. Zhu, et al., Sca1(+) cells minimally contribute to smooth muscle cells in atherosclerosis, Circ. Res. 128 (2021) 133–135, https://doi.org/10.1161/circresaha.120.317972.

[8] L.C. Steffes, A.A. Froistad, A. Andruska, et al., A notch3-marked subpopulation of vascular smooth muscle cells is the cell of origin for occlusive pulmonary vascular lesions, Circulation 142 (2020) 1545–1561, https://doi.org/10.1161/circulationaha.120.045750.

[9] C. Wilson, C.D. Saunter, J.M. Girkin, et al., Clusters of specialized detector cells provide sensitive and high fidelity receptor signaling in the intact endothelium, Faseb. J. 30 (2016) 2000–2013, https://doi.org/10.1096/fj.201500090.

[10] J.F. Bentzon, M.W. Majesky, Lineage tracking of origin and fate of smooth muscle cells in atherosclerosis, Cardiovasc. Res. 114 (2018) 492–500, https://doi.org/10.1093/cvr/cvx251.

[11] G.L. Basatemur, H.F. Jørgensen, M.C.H. Clarke, et al., Vascular smooth muscle cells in atherosclerosis, Nat. Rev. Cardiol. 16 (2019) 727–744, https://doi.org/10.1038/s41569-019-0227-9.

[12] C.E. Hart, A.W. Clowes, Platelet-derived growth factor and arterial response to injury, Circulation 95 (1997) 555–556, https://doi.org/10.1161/01.cir.95.3.555.

[13] J. Thyberg, K. Blomgren, J. Roy, et al., Phenotypic modulation of smooth muscle cells after arterial injury is associated with changes in the distribution of laminin and fibronectin, J. Histochem. Cytochem. 45 (1997) 837–846, https://doi.org/10.1177/002215549704500608.

[14] N. Mendez-Barbero, C. Gutierrez-Munoz, L.M. Blanco-Colio, Cellular crosstalk between endothelial and smooth muscle cells in vascular wall remodeling, Int. J. Mol. Sci. 22 (2021), https://doi.org/10.3390/ijms22147284.

[15] B. Hinz, The extracellular matrix and transforming growth factor-β1: tale of a strained relationship, Matrix Biol. 47 (2015) 54–65, https://doi.org/10.1016/j.matbio.2015.05.006.

[16] S. Kijani, A.M. Vazquez, M. Levin, et al., Intimal hyperplasia induced by vascular intervention causes lipoprotein retention and accelerated atherosclerosis, Phys. Rep. 5 (2017), e13334, https://doi.org/10.14814/phy2.13334.

[17] D.G. Kuhel, B. Zhu, D.P. Witte, et al., Distinction in genetic determinants for injury-induced neointimal hyperplasia and diet-induced atherosclerosis in inbred mice, Arterioscler. Thromb. Vasc. Biol. 22 (2002) 955–960, https://doi.org/10.1161/01.atv.0000017994.77066.75.

[18] C. Yap, A. Mieremet, C.J.M. de Vries, et al., Six shades of vascular smooth muscle cells illuminated by KLF4 (Krüppel-Like factor 4), Arterioscler. Thromb. Vasc. Biol. 41 (2021) 2693–2707, https://doi.org/10.1161/atvbaha.121.316600.

[19] E. Miguel-Velado, F.D. Pérez-Carretero, O. Colinas, et al., Cell cycle-dependent expression of Kv3.4 channels modulates proliferation of human uterine artery smooth muscle cells, Cardiovasc. Res. 86 (2010) 383–391, https://doi.org/10.1093/cvr/cvq011.

[20] A. Misra, Z. Feng, R.R. Chandran, et al., Integrin beta3 regulates clonality and fate of smooth muscle-derived atherosclerotic plaque cells, Nat. Commun. 9 (2018) 2073, https://doi.org/10.1038/s41467-018-04447-7.

[21] A.W. Clowes, M.A. Reidy, M.M. Clowes, Kinetics of cellular proliferation after arterial injury. I. Smooth muscle growth in the absence of endothelium, Lab. Invest. 49 (1983) 327–333.

[22] I. Kabir, X. Zhang, J.M. Dave, et al., The age of bone marrow dictates the clonality of smooth muscle-derived cells in atherosclerotic plaques, Nat Aging 3 (2023) 64–81, https://doi.org/10.1038/s43587-022-00342-5.

[23] J.B. Kim, Q. Zhao, T. Nguyen, et al., Environment-sensing aryl hydrocarbon receptor inhibits the chondrogenic fate of modulated smooth muscle cells in atherosclerotic lesions, Circulation 142 (2020) 575–590, https://doi.org/10.1161/circulationaha.120.045981.

[24] T. Warwick, G.K. Buchmann, B. Pflüger-Müller, et al., Acute injury to the mouse carotid artery provokes a distinct healing response, Front. Physiol. 14 (2023), 1125864, https://doi.org/10.3389/fphys.2023.1125864.

[25] C. Bramlett, D. Jiang, A. Nogalska, et al., Clonal tracking using embedded viral barcoding and high-throughput sequencing, Nat. Protoc. 15 (2020) 1436–1458, https://doi.org/10.1038/s41596-019-0290-z.